

Discovery of *N*-{1-[3-(3-Oxo-2,3-dihydrobenzo[1,4]oxazin-4-yl)propyl]piperidin-4-yl}-2-phenylacetamide (Lu AE51090): An Allosteric Muscarinic M₁ Receptor Agonist with Unprecedented Selectivity and Procognitive Potential

Anette G. Sams,^{*,†} Morten Hentzer,[‡] Gitte K. Mikkelsen,[†] Krestian Larsen,[†] Christoffer Bundgaard,[§] Niels Plath,^{||} Claus T. Christoffersen,[‡] and Benny Bang-Andersen[†]

[†]Medicinal Chemistry Research, [‡]Molecular Pharmacology, [§]Discovery ADME, and ^{||}In Vivo Neuropharmacology, Lundbeck Research Denmark, H. Lundbeck A/S, Ottiliavej 9, DK-2500 Valby, Denmark

Received June 10, 2010

The discovery and structure–activity relationship (SAR) of a series of allosteric muscarinic M₁ receptor agonists are described. Compound **17** (Lu AE51090) was identified as a representative compound from the series, based on its high selectivity as an agonist at the muscarinic M₁ receptor across a panel of muscarinic receptor subtypes. Furthermore, **17** displayed a high degree of selectivity when tested in a broad panel of G-protein-coupled receptors, ion channels, transporters, and enzymes, and **17** showed an acceptable pharmacokinetic profile and sufficient brain exposure in rodents in order to characterize the compound in vivo. Hence, in a rodent model of learning and memory, **17** reversed delay-induced natural forgetting, suggesting a procognitive potential of **17**.

Introduction

Muscarinic (M) acetylcholine (ACh^a) receptors are members of superfamily A of the G-protein-coupled receptors (GPCRs) and mediate the action of the neurotransmitter ACh in the peripheral and central nervous system (CNS). Five muscarinic receptor subtypes (M₁–M₅) have been cloned. The M₁, M₃, and M₅ receptors couple to G_{q/11}, and their stimulation leads to activation of phospholipase C and increase in phosphoinositol (PI) turnover, resulting in intracellular calcium release. The M₂ and M₄ receptors mediate their signaling via G_{i/o}, and activation of these subtypes leads to reduced cAMP production through inhibition of adenylate cyclase activity.¹

The M₁ receptor is the predominant muscarinic receptor subtype in the CNS and is located in brain areas such as cerebral cortex and hippocampus. These brain areas are important for learning and memory, and activation of M₁ receptors has been suggested to mediate higher cognitive processing. Moreover, these brain regions are severely affected by cholinergic dysfunction in Alzheimer's disease (AD),

from early stages and onward.^{2,3} A central role for the M₁ receptor in cognition was first demonstrated in mouse M₁ receptor knockout studies, where M₁ ^{−/−} mice revealed deficits in hippocampus and prefrontal cortex dependent working and episodic memory tasks.^{4,5} In addition, M₁ receptor expression is decreased in cortical regions of schizophrenia patients, although this has not yet been linked to a functional outcome.^{6,7} Hence, it has been suggested that M₁ receptor agonism has a role in the treatment of AD and cognitive impairment associated with schizophrenia (CIAS).^{8–11}

During the 1990s, several pharmaceutical companies pursued selective muscarinic M₁ receptor agonists as potential therapeutics for the treatment of AD and schizophrenia. While many of the compounds were efficacious in preclinical animal models of cognitive dysfunction, those compounds that were progressed into clinical studies were dose limited by various adverse effects, including vomiting, nausea, and sweating, which prohibited their use in clinical practice of AD treatment.¹² However, in clinical studies **1**¹³ (Chart 1) demonstrated an effect on cognitive and behavioral symptoms in AD patients,^{14,15} and on measures of verbal learning and short-term memory functions in schizophrenic patients.¹⁶ Many of the first generation M₁ receptor agonists were invented on the basis of structures of naturally occurring, nonselective muscarinic receptor agonists, such as arecholine.^{17,18} The moderate selectivity of these compounds for M₁ receptors over the other muscarinic receptor subtypes, especially M₂ and M₃ receptors,^{8,12,18} has been suggested to be the cause of the observed peripheral cholinergic side effects.

The modest selectivity of the first generation M₁ receptor agonists has been suggested to be a direct consequence of these compounds activating the M₁ receptor through orthosteric regions, which display a high level of sequence homology among the subtypes of the muscarinic receptor family.

*To whom correspondence should be addressed. Current address: LEO Pharma A/S, Industriparken 55, DK-2750 Ballerup, Denmark. Phone: +45 44945888. Fax: +45 72263320. E-mail: anette.sams@leo-pharma.com

^a Abbreviations: SAR, structure–activity relationship; AD, Alzheimer's disease; CNS, central nervous system; ADME, absorption, distribution, metabolism, excretion; AUC, area under the curve; iv, intravenous; ITI, intertrial interval; CHO, Chinese hamster ovary; BHK, baby hamster kidney; PI, phosphoinositol; GPCR, G-protein-coupled receptor; ACh, acetylcholine; CCh, carbachol; SPA, scintillation proximity assay; HEPES, 4-(2-hydroxyethyl)-1-piperazineethanesulfonic acid; EDTA, ethylenediaminetetraacetic acid; SCX, strong cation exchange; DMF, dimethylformamide; THF, tetrahydrofuran; DIPEA, diisopropylethylamine; TFA, trifluoroacetic acid; CDI, carbonyl diimidazole; MTBD, 7-methyl-1,5,7-triazabicyclo[4.4.0]dec-5-ene; LC/MS–MS, liquid chromatography–tandem mass spectrometry; ELSD, evaporative light scattering detection.

Spalding et al. reported the discovery of an allosteric muscarinic M₁ receptor agonist **2** (AC-42)¹⁹ belonging to a novel structural class of muscarinic receptor agonists. It was shown that **2** displayed complete selectivity as an agonist of the M₁ receptor versus the other muscarinic receptor subtypes. Mutagenesis and pharmacological studies later revealed that this compound activates the muscarinic M₁ receptor with a mode of action different from that of orthosteric muscarinic receptor agonists.^{20,21}

The discovery of allosteric M₁ receptor agonists spurred a renewed interest in the muscarinic field, and a number of allosteric agonists of the M₁ receptor have since appeared. These second generation muscarinic M₁ receptor agonists have a potential for subtype selectivity, since they activate the receptor through interaction with less conserved regions among the muscarinic receptor subtypes. Subsequent to the discovery of **2**, other compounds have been reported as allosteric agonists of the muscarinic M₁ receptor, such as **3**

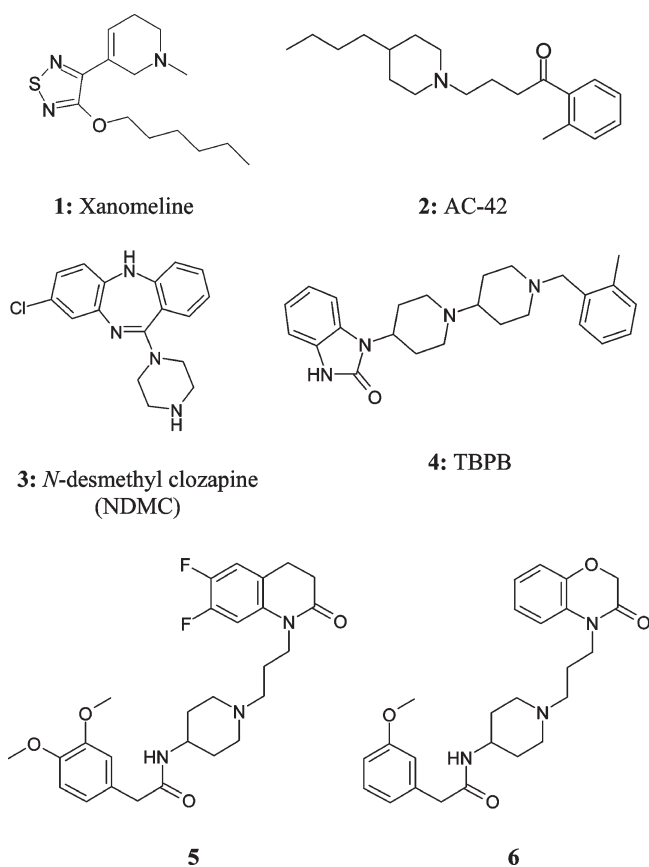
(NDMC),²² a metabolite of the atypical antipsychotic drug clozapine, and more recently **4** (TBPB)²³ was reported.

A small screening campaign was conducted in our laboratory to identify allosteric muscarinic M₁ receptor agonists using a functional Ca²⁺ flux assay. Here, we report the discovery of **5** and a related analogue **6** and their development into a novel series of allosteric M₁ receptor agonists. From this series, the allosteric M₁ receptor partial agonist **17** (Lu AE51090) was selected and further characterized. In short, **17** displayed unprecedented selectivity for the muscarinic M₁ receptor versus other muscarinic receptor subtypes, when assayed for functional agonism and in binding assays. Compound **17** also displayed high selectivity when tested in a panel of 69 receptors, ion channels, transporters, and enzymes. Also, **17** had suitable pharmacokinetic properties and was active in an in vivo model of working memory, making it a high quality lead compound for a drug discovery program.

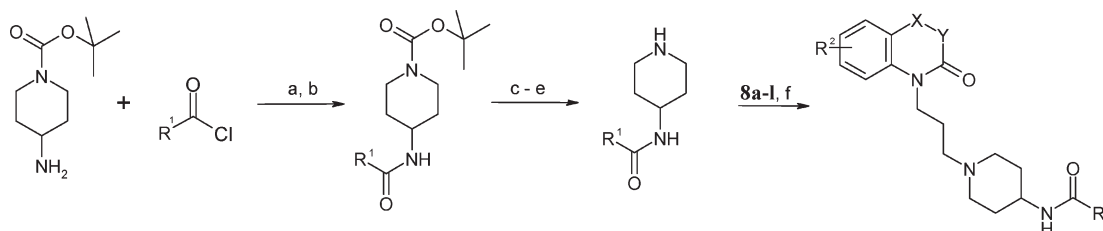
Chemistry

A parallel synthesis protocol was developed in order to explore the SAR of the two initial hits **5** and **6** in a rapid manner, as outlined in Scheme 1. Commercially available *tert*-butyl 4-aminopiperidine-1-carboxylate was acylated with an excess of a suitable carboxylic acid chloride in the presence of TBD-methylpolystyrene, a polymer immobilized version of the organic base 7-methyl-1,5,7-triazabicyclo[4.4.0]dec-5-ene (MTBD), to drive the acylation reaction to completion. The residual carboxylic acid chloride was removed by the addition of tris-(2-aminoethyl)amine polystyrene as a scavenger. The resins were subsequently removed by filtration, and the resulting crude product was deprotected by addition of trifluoroacetic acid to the solution. The solvent was evaporated and the residue redissolved in MeOH and loaded onto a sulfonic acid based strong-cation-exchange (SCX) column. The loaded SCX column was washed repeatedly with MeOH and acetonitrile to remove nonbasic impurities, and the adsorbed piperidin-4-ylcarboxamide was subsequently eluted by rinsing the column with 4 M NH₃ in MeOH. The fractions containing the product were evaporated and redissolved in DMF and finally alkylated with the intermediates **8a–l** in the presence of DIPEA. By this protocol, compounds **6**, **9–16**, **18–20**, **22–32**, **34**, and **35** were obtained. The intermediate **8l** was commercially available, while intermediates **8a–k** were prepared as described in Scheme 2. Thus, suitably substituted 4*H*-benzo[1,4]oxazin-3-ones **7a,j** or 3,4-dihydro-1*H*-quinolin-2-ones **7b–i** and 4*H*-benzo[1,4]thiazin-3-one **7k** were deprotonated with NaH and alkylated with 1,3-dibromopropane or 1-bromo-3-chloropropane, as specified in Scheme 2. The intermediates **7a,b,d–f,h,i,k** were commercially available, while **7c**, **7g**, and **7j** were prepared as outlined in Scheme 3.

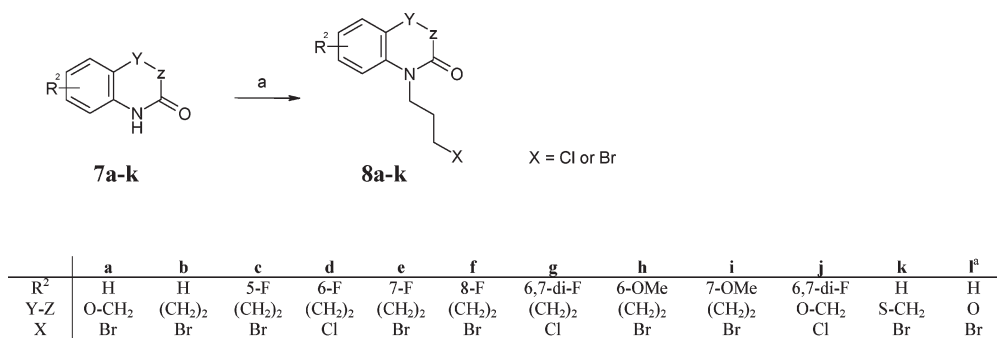
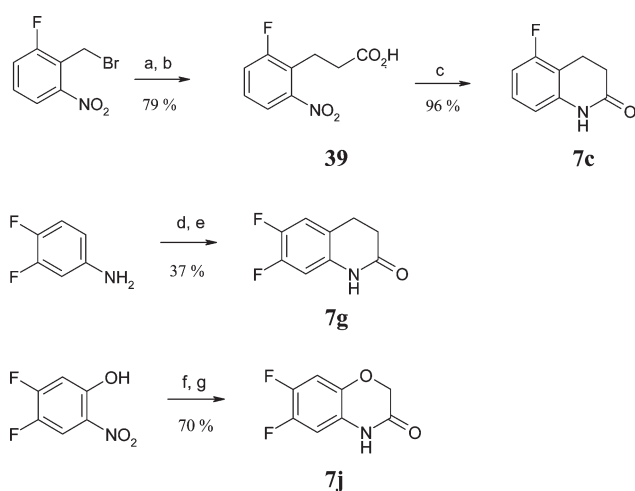
Chart 1. Structures of Muscarinic Agonists



Scheme 1. Parallel Synthesis Protocol to Prepare Analogues of **5**^a



^a(a) TBD-methylpolystyrene, 1,2-dichloroethane; (b) Tris-(2-aminoethyl)amine polystyrene resin; (c) TFA; (d) SCX resin; (e) NH₃/MeOH (4 M); (f) DIPEA, DMF.

Scheme 2. Preparation of Intermediates 8a–k^a^a Commercial source^a (a) NaH, Br(CH₂)₃X, DMF.Scheme 3. Preparation of Intermediates 7c, 7g, and 7j^a

^a (a) Diethyl malonate, NaH, DMF; (b) AcOH, HCl, reflux; (c) 10% Pd/C, HCOONH₄, MeOH, reflux; (d) 3-chloropropionyl chloride, DIPEA, ethyl acetate; (e) AlCl₃, 180 °C; (f) 5% Pd/C, H₂, EtOH; (g) chloroacetyl chloride, K₂CO₃, DMF.

2-Fluoro-6-nitrobenzyl bromide was reacted with diethyl malonate, followed by diethyl ester hydrolysis and subsequent decarboxylation of one of the carboxy groups to give **39** in 79% yield. The nitro group of **39** was reduced to give the corresponding aniline, which was subsequently cyclized to give **7c** in 96% yield. The intermediate **7g** was prepared by acylating 3,4-difluoroaniline with 3-chloropropionyl chloride followed by a Friedel–Crafts alkylation to effect ring closure in 37% overall yield. Intermediate **7j** was obtained by reduction of 4,5-difluoro-2-nitrophenol to the corresponding aniline followed by reaction with chloroacetyl chloride in 70% overall yield. A slight modification of the procedure outlined in Scheme 1, with simple permutations of the individual steps as described in the Experimental Section, was adopted for the larger scale preparations of compounds **5**, **17**, **33**, and **36–38**.

Biological Evaluation

Biological in vitro assays were employed to determine the pharmacological activity of the compounds and to establish a SAR. Agonist potency (EC₅₀) and efficacy (E_{max}) at the human muscarinic M₁–M₅ receptors was assayed in func-

tional Ca²⁺ mobilization assays using stably transfected Chinese hamster ovary (CHO-K1) cells, expressing the human M₁ or M₂ receptor, or using baby hamster kidney (BHK-21) cells, expressing the human M₃, M₄, or M₅ receptor. The cell lines expressing the human M₂ or M₄ receptor coexpressed the promiscuous G_{α16} subunit. Agonist evoked increases in intracellular Ca²⁺ was measured by fluorometric imaging. Concentration–response data were fitted to the four-parameter logistic equation to estimate compound potency and efficacy of test compounds.²⁴

Binding affinities at human muscarinic M₂–M₅ receptors were determined by tritium-labeled radioligand binding to membrane preparations from cell lines expressing the respective human muscarinic receptors, using a scintillation proximity assay (SPA) and the radioligands [³H]AFDX-384 (M₂) and [³H]4-DAMP (M₃–M₅).

In Vitro and in Vivo ADME Evaluation

A range of in vitro and in vivo assays were employed to assess the ADME properties of the compounds and to predict the pharmacokinetic properties in humans. The metabolic stability was investigated in cryopreserved hepatocytes of rat and human origin. The first-order elimination rate constant for disappearance of parent compound was calculated from the slope of the logarithm of the transformed concentration–time curve. Plasma protein binding was determined in vitro in rat and human plasma following incubation and ultracentrifugation. In vivo pharmacokinetics were studied in rats following single intravenous (1 mg/kg) and oral (2 mg/kg) administration of compounds. Serial blood samples were collected at various time points up to 6 h after dosing. In vivo pharmacokinetic parameters were obtained following compartmental modeling. The extent of brain penetration was examined in rats and mice following single subcutaneous administration. Animals were anesthetized at different time points, and cardiac blood was obtained followed by decapitation and homogenization of the brain. Bioanalysis of samples from all in vitro and in vivo ADME assays was performed by liquid chromatography–tandem mass spectrometry (LC/MS–MS).

Prediction of hepatic clearance in humans was done by in vitro/in vivo extrapolation from the predicted hepatic clearance in rats and humans according to the well-stirred model²⁵ and the observed systemic in vivo clearance in rats.²⁶

Table 1. Functional Agonism at Muscarinic M₁–M₅ Receptors^a

compd	hM ₁		hM ₂		hM ₃		hM ₄		hM ₅	
	EC ₅₀ (nM)	E _{max} (%)	EC ₅₀ (nM)	E _{max} (%)	EC ₅₀ (nM)	E _{max} (%)	EC ₅₀ (nM)	E _{max} (%)	EC ₅₀ (nM)	E _{max} (%)
ACh	1.1	100	220	100	3.2	100	10	100	1.2	100
17	61	83		0% at 10 μM		1% at 10 μM		6% at 10 μM		1% at 10 μM
1	1.6	89		9% at 10 μM	120	54	6.2	72	140	60
2	150	87		1% at 10 μM		6% at 10 μM		2% at 10 μM		4% at 10 μM
3	18	75		3% at 10 μM		10% at 10 μM	400	12	170	34
4	6.5	86	nd	nd		1% at 10 μM		38% at 10 μM		5% at 10 μM
5	13	91		2% at 10 μM		7% at 10 μM	300	48	1200	52
6	130	86		0% at 10 μM		0% at 10 μM		3% at 10 μM		6% at 10 μM

^aData are the mean of three experiments. Percent activity at the indicated concentration is given when an EC₅₀ could not be established. nd: not determined.

Results and Discussion

A screening campaign covering approximately 10 000 compounds led to the discovery of the potent M₁ receptor agonist **5** and its close analogue **6**. The screen was performed using a Ca²⁺ mobilization based functional assay with a stably transfected Chinese hamster ovary (CHO-K1) cell line expressing the human M₁ receptor. In this assay, **5** had an EC₅₀ of 13 nM and an efficacy (E_{max}) of 91% relative to the endogenous muscarinic agonist ACh while **6** was a partial agonist with an EC₅₀ of 130 nM and an E_{max} of 86% relative to ACh. The reference compound ACh had an EC₅₀ of 1.1 nM, and the E_{max} was defined to 100%.

Hit compounds **5** and **6** were also tested for agonism at the muscarinic M₂–M₅ receptors (Table 1). Compound **5** displayed no agonist activity at the M₂ and M₃ receptors, while it was a moderately potent partial agonist at the M₄ receptor (EC₅₀ = 300 nM, E_{max} = 48%) as well as a weak partial agonist at the M₅ receptor (EC₅₀ = 1200 nM, E_{max} = 52%). In contrast, compound **6** showed no agonist activity at any of the M₂–M₅ receptors.

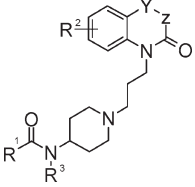
A series of analogues of **5** and **6** was prepared, and their potencies and efficacies at the M₁ receptor are summarized in Table 2. The aim was initially to investigate the contribution of the substituents of the highly decorated scaffold of **5** to the M₁ receptor activity of the compound. Surprisingly, removal of the two benzylic methoxy substituents led to an equipotent compound **9**. We subsequently examined the individual effects of fluorine substituents at the aromatic positions of the tetrahydroquinolinone ring system (**10**–**13**). The monofluorinated isomers were all less potent than **9**. In particular, compounds **10** and **13** with monofluoro substituents at the 5- or 8-position were approximately 10- to 20-fold weaker when compared to **9**, while compounds **11** and **12** with monofluoro substituents at the 6- or 7-position were only marginally weaker than **9**. Replacing the fluoro substituents of compounds **11** and **12** with methoxy substituents led to a loss of activity, while the fully unsubstituted compound **16** was equipotent to **11** and **12**. The corresponding benzoxazinone derivative **17** was equipotent to the tetrahydroquinolinone derivative **16**, while the benzothiazinone derived analogue **18** was slightly less potent than **16** and the corresponding benzoxazolone derivative **19** even less potent. Compound **17** was subsequently used as the reference for further SAR work around the benzoxazolone scaffold. Thus, methylation of the amide functionality resulted in a substantial loss of M₁ receptor agonism (compound **20**), and reversing the amide, as in **21** (Figure 1), resulted in an inactive compound. We also explored the effects of changing the amide substituent of **17**, and replacing the benzyl group of **17** with a phenyl substituent completely removed M₁ receptor agonist activity, as exempli-

fied with compound **22**. Also, extending the linker between the carbonyl and phenyl ring as in compound **23** was unfavorable. However, replacing the benzyl group of **17** with a methyl group (compound **24**) only led to a modest 3-fold drop in potency compared to **17**, and the corresponding ethyl analogue almost restored the M₁ receptor potency to the level of **5**, yet with significantly less molecular mass ($\Delta M = 156$ Da) (**25**). Other small alkyl substituents at the amide yielded compounds that were less potent at the M₁ receptor (**25**–**31**) compared to **25**, and R¹ = isobutyl (**27**) or cyclohexyl (**31**) gave compounds devoid of M₁ receptor agonism. Interestingly, while all other compounds in the series were partial muscarinic M₁ receptor agonists with relatively high efficacy in the range of 70–90% relative to ACh, compounds **29** and **30**, wherein R¹ = cyclobutyl and cyclopentyl, respectively, were partial M₁ receptor agonists with significantly lower E_{max} of approximately 40% relative to ACh.

We repeated the fluoro scan of the aromatic positions of the tetrahydroquinolinone ring system, leading to the ethyl amide derivatives **32**–**35**. As was seen for the benzyl substituted amide analogues, a fluorine substituent at the 8-position was unfavorable as exemplified by compounds **35** and **13**. However, introducing a fluorine atom at the 5-, 6-, or 7-position yielded largely equipotent compounds, but in this case the 6,7-difluoro substitution pattern did not appear to give a synergistic effect in contrast to what was seen with the benzylic amide substituent (**34**–**36** versus **9**, **11**, **12**). Compounds **32**–**34**, **36**, and **38** were among the most potent compounds of the series, displaying EC₅₀ values between 10 and 20 nM corresponding to the level of compound **5**. Also, in this case, the corresponding methyl analogue **37** was less potent than the ethyl analogue **36**. In analogy with the benzylamide series, the ethylamide derivative of the 6,7-difluoro substituted benzoxazinone based scaffold (**38**) was equipotent to the tetrahydroquinolinone-based analogue **36**.

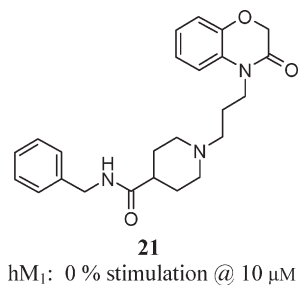
The hit compound **5** displayed a mixed agonistic profile at the M₁, M₄, and M₅ receptors; hence, we monitored the selectivity of selected compounds of the series versus other muscarinic receptor subtypes. It was discovered that the agonistic effects at the M₄ and M₅ receptors observed for **5** were related to the 3,4-dimethoxy substitution pattern at the benzylic amide substituent, and agonism at M₂–M₅ was generally not observed in any of the compounds of the series when this substitution pattern was avoided (data not shown).

Compound **17** was identified as a highly selective M₁ receptor agonist versus M₂–M₅ and was selected early on as a prototype compound for in-depth profiling and as a benchmark to reference compounds. The fact that a compound does not elicit an agonist response at a receptor does not exclude the possibility that the compound may show antagonistic effects

Table 2. Functional M₁ Structure–Activity Relationship for a Series of Analogues of **5** and **6**^a


compd	R ¹	R ²	R ³	Y–Z	hM ₁	
					EC ₅₀ (nM)	E _{max} (%)
5	(3,4-di-OMe)benzyl	6,7-di-F	H	CH ₂ –CH ₂	13	91
6	(3-OMe)benzyl	H	H	O–CH ₂	130	86
9	benzyl	6,7-di-F	H	CH ₂ –CH ₂	15	89
10	benzyl	5-F	H	CH ₂ –CH ₂	150	77
11	benzyl	6-F	H	CH ₂ –CH ₂	49	79
12	benzyl	7-F	H	CH ₂ –CH ₂	51	86
13	benzyl	8-F	H	CH ₂ –CH ₂	290	75
14	benzyl	6-OMe	H	CH ₂ –CH ₂	560	84
15	benzyl	7-OMe	H	CH ₂ –CH ₂	120	83
16	benzyl	H	H	CH ₂ –CH ₂	48	89
17	benzyl	H	H	O–CH ₂	61	83
18	benzyl	H	H	S–CH ₂	100	79
19	benzyl	H	H	O	1100	70
20	benzyl	H	Me	O–CH ₂	910	67
22	phenyl	H	H	O–CH ₂	nd	8% at 10 μM
23	(2-phenyl)ethyl	H	H	O–CH ₂	970	60
24	methyl	H	H	O–CH ₂	180	74
25	ethyl	H	H	O–CH ₂	27	78
26	isopropyl	H	H	O–CH ₂	46	72
27	isobutyl	H	H	O–CH ₂	nd	21% at 10 μM
28	cyclopropyl	H	H	O–CH ₂	110	74
29	cyclobutyl	H	H	O–CH ₂	160	37
30	cyclopentyl	H	H	O–CH ₂	350	41
31	cyclohexyl	H	H	O–CH ₂	nd	3% at 10 μM
32	ethyl	5-F	H	CH ₂ –CH ₂	19	90
33	ethyl	6-F	H	CH ₂ –CH ₂	9	83
34	ethyl	7-F	H	CH ₂ –CH ₂	20	83
35	ethyl	8-F	H	CH ₂ –CH ₂	310	78
36	ethyl	6,7-di-F	H	CH ₂ –CH ₂	20	87
37	methyl	6,7-di-F	H	CH ₂ –CH ₂	86	76
38	ethyl	6,7-di-F	H	O–CH ₂	10	88

^aData are the mean of three experiments. When an EC₅₀ could not be established, activity is given as the percent activity at the concentration indicated. nd: not determined.

**Figure 1.** Inverted amide analogue of **17**.

at the receptor, for instance, by binding to inactive receptor conformations. Therefore, we studied the binding of compound **17** to M₂–M₅ receptors (Table 3) using orthosteric antagonist radioligands and benchmarked to reference compounds. Among the compounds tested, **17** displayed the least binding to the muscarinic receptor subtypes M₂–M₅, making it uniquely selective for the M₁ receptor. In comparison, **1**, a classical orthosteric M₁ receptor agonist, caused partial activation of the M₄ receptor and, to a lesser extent, activation of

Table 3. Binding Affinities at Muscarinic M₂–M₅ Receptors^a

compd	K _i (nM)			
	hM ₂	hM ₃	hM ₄	hM ₅
atropine	1.9	0.9	3.0	1.0
17	2200	7000	6900	8900
1	120	13	72	80
2	980	2800	1400	4500
3	250	90	290	51
4	320	430	130	940

^aData are means of three experiments.

M₃ and M₅ receptors as well as binding affinity for the M₂ receptor. Indeed, it has been hypothesized that the M₄ receptor agonism of this compound is responsible for its effects on positive symptoms of schizophrenia.²⁷ Furthermore, **3** showed partial agonism at the M₅ receptor and binding affinity for several muscarinic receptors, suggesting that **3** has a complex muscarinic pharmacology with mixed agonism and antagonism at different receptor subtypes. Compound **2** only displayed agonistic activity at the M₁ receptor and weak binding affinity for the M₂–M₅ receptors. Recently, **4** was disclosed as a potent and highly subtype selective allosteric M₁

receptor agonist.²⁸ In our hands, **4** showed no agonistic effects at other muscarinic receptors than the M_1 , but the compound did exhibit moderately potent binding affinities at the M_2 – M_4 receptors (Table 3).

Characterization of Mode of Action of Compound 17 at the M_1 Receptor. Ca^{2+} mobilization is a distal event in the signaling cascade triggered by M_1 receptor activation, and several signaling pathways converge at the point of calcium release. Therefore, we wanted to validate that the observed compound effects were specifically mediated by activation of

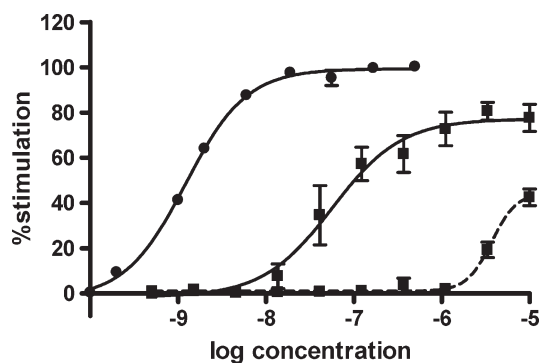


Figure 2. Concentration-dependent stimulation of Ca^{2+} mobilization in CHO-hM1 cells by ACh (circles) and **17** (squares, solid line). Antagonism of response to **17** by 100 nM atropine (squares, dashed line). Data are the mean of three experiments (\pm SEM).

the muscarinic M_1 receptor. Compound **17** did not elicit a Ca^{2+} mobilization response when assayed on the parental CHO cell line (i.e., not expressing the M_1 receptor; data not shown). The response of the M_1 receptor expressing CHO cell line to **17** was antagonized by atropine, a competitive muscarinic antagonist, hence demonstrating that the response **17** was specifically mediated by the M_1 receptor, as shown in Figure 2.

Classical orthosteric agonists display no saturability in the interaction with an orthosteric antagonist; i.e., the dose–response curves can be right-shifted indefinitely by increasing concentrations of the agonist and antagonist. In a Schild regression plot, this will translate into a slope of unity for orthosteric interaction. Conversely, the action of an allosteric agonist is characterized by saturability of the interaction with an orthosteric antagonist. This relationship translates into a slope that deviates from unity.^{21,29} In such a competitive antagonist assay, compound **17** behaved unlike classical orthosteric agonists like ACh and carbachol (CCh) but competed with atropine in a fashion consistent with an allosteric mode of M_1 receptor activation. The results for **17** were comparable to those obtained for the allosteric M_1 receptor agonist **2** (Figure 3).

In order to further validate the allosteric mode of M_1 receptor activation by **17**, the compound was assayed for activity at the Y381A mutant M_1 receptor,¹⁹ in which the essential tyrosine residue 381 located in the transmembrane

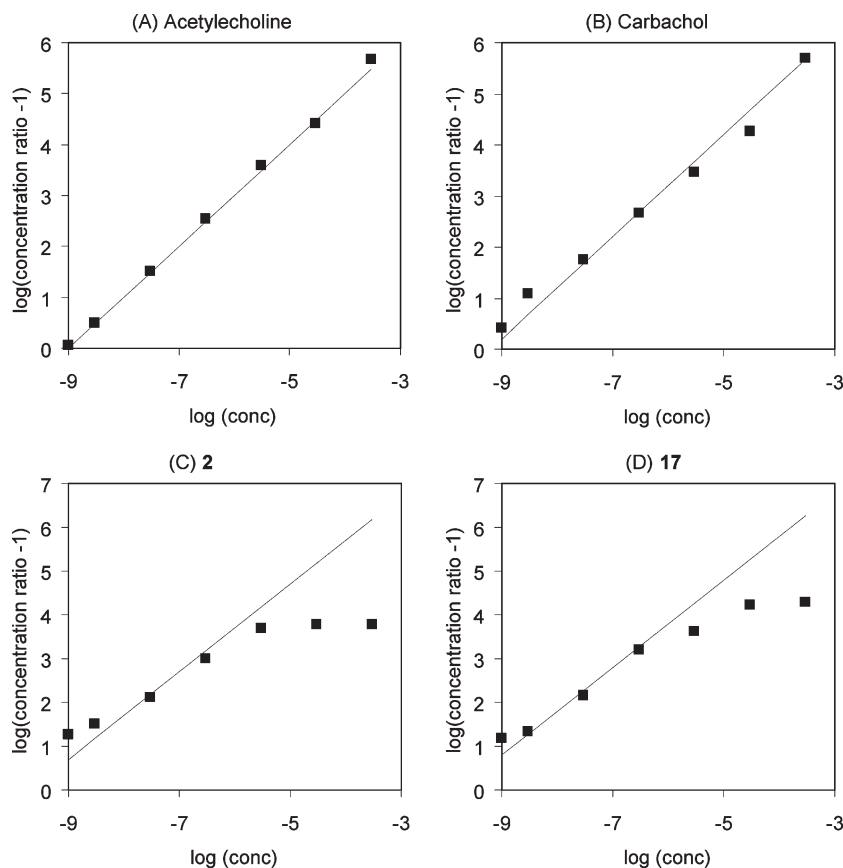


Figure 3. Detection of allosteric agonism by Schild regression: Schild regression for the interaction between the orthosteric antagonist atropine and (A) the orthosteric agonist ACh, (B) the orthosteric agonist carbachol, (C) the allosteric agonist **2**, and (D) compound **17**. Data are from a cell-based Ca^{2+} assay. The dashed lines represent a theoretical Schild regression of unit slope as expected for simple competitive antagonism by atropine. In the experiments with acetylcholine and carbachol, the 95% confidence interval of the slope factor included the unit slope, and the $-pK_b$ for atropine was in the range 9.0–9.6 and, hence, in agreement with literature values (www.iuphar-db.org). Shown are representative data from three independent experiments.

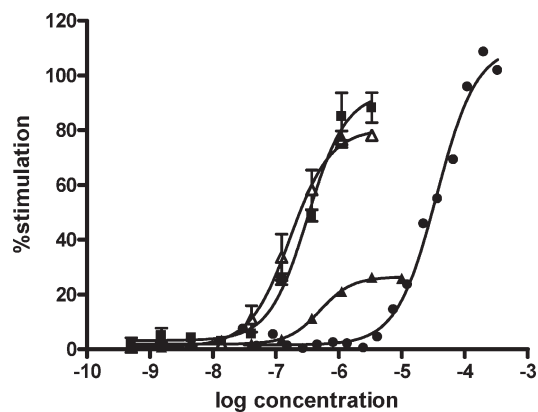


Figure 4. Concentration-dependent stimulation of Ca^{2+} mobilization in CHO-K1 hM1-Y381A cells by acetylcholine (solid circles; $\text{EC}_{50} = 27000$ nM, $E_{\text{max}} = 100\%$), **17** (solid squares; $\text{EC}_{50} = 97$ nM; $E_{\text{max}} = 82\%$), **2** (solid triangles; $\text{EC}_{50} = 500$ nM, $E_{\text{max}} = 31\%$), and **3** (open triangles, $\text{EC}_{50} = 140$ nM; $E_{\text{max}} = 72\%$). Data are the mean of three experiments (\pm SEM).

Table 4. List of Target Affinities for Which a $K_i < 1000$ nM Was Obtained from a Panel Screen of **17** and **2** on 69 Receptors, Ion Channels, Transporters, and Enzymes^a

Receptor (K_i ; nM)	Compound	
	17	2
h α_{1A}	260	18
h α_{1B}	910	65
h α_{1D}		40
h α_{2A}		530
h α_{2B}		840
hD ₂		77
hD ₄		11
hH ₁	780	610
5-HT _{1A}		280

^aData are the mean of two determinations.

domain 6 is mutated to alanine. The Y381 residue contributes to the orthosteric binding site of the M_1 receptor, and mutation to alanine has been shown to decrease acetylcholine binding affinity 30-fold and drastically reduce its potency about 3000-fold without affecting efficacy.³⁰ The critical contribution of Y381 to the orthosteric site of the M_1 receptor makes the Y381A M_1 receptor mutant a useful tool to detect allosteric agonists. We verified that the Y381A M_1 receptor mutant showed greatly reduced potency with ACh (20000-fold reduction) and CCh, as shown in Figure 4. To the contrary, the allosteric M_1 receptor agonists **2** and **3** showed only minor changes in potency (2-fold reduction and 7-fold increase, respectively), which is in agreement with published results.^{19,30} Compound **17** showed unaltered potency and efficacy at the Y381A M_1 receptor compared to the wild-type M_1 receptor. These data suggest that compound **17** interacts with the M_1 receptor in a different mode than ACh and, hence, is an allosteric M_1 receptor agonist.

Broad Selectivity Profiling. Compounds **17** and **2** were the two most selective allosteric M_1 receptor agonists and were tested in a broad pharmacology panel screen against 69 receptors, ion channels, transporters, and enzymes. The targets for which **17** and **2** showed high to medium affinity ($K_i < 1000$ nM) are listed in Table 4. Compound **17** only displayed minor cross-reactivity with other targets, and the most predominant effect was the affinity for the adrenergic α_{1A} receptor, at which **17** had a K_i of 260 nM. In contrast, **2**

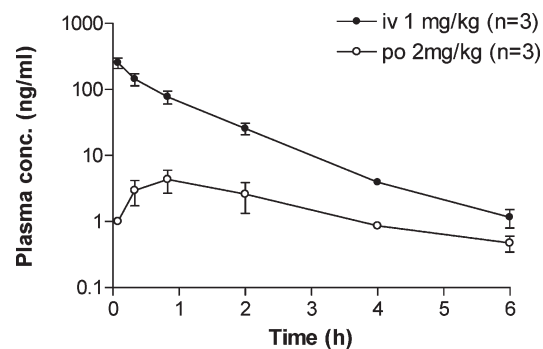


Figure 5. Plasma concentration–time plots of **17** following intravenous (1 mg/kg) and oral (2 mg/kg) administration in Sprague–Dawley rats. Data shown are the mean \pm SD ($n = 3$).

Table 5. Main Pharmacokinetic Parameters of **17** after Intravenous (1 mg/kg) and Oral (2 mg/kg) Administration in Rats^a

CL_p ((L/h)/kg)	$t_{1/2}, \beta$ (h)	V_{ss} (L/kg)	T_{max} (po) (h)	F (po) (%)
5.0 ± 0.9	0.8 ± 0.06	4.8 ± 0.9	0.8 ± 0.1	4.0 ± 1.7

^aValues shown are the average \pm SD ($n = 3$).

displayed a broader pharmacological profile, with affinity to several targets, such as α_1 , dopamine D₂ and D₄, and serotonin 5-HT_{1A} receptors. Thus, the pharmacological profile of **2** at receptors other than the muscarinic receptor family, in particular such as D₂ but also α_1 receptors, makes it less suitable for use as a tool to study in vivo pharmacological effects of M_1 receptor agonism in in vivo models of schizophrenia. In addition to profiling across the muscarinic M_2 – M_5 receptors (Table 3), **4** was tested in a smaller panel of nine GPCRs of the dopaminergic, histaminergic, adrenergic, and serotonergic receptor families and found to possess α_1 and 5-HT_{2C} receptor affinity (for $\alpha_{1A,B,D}$, $K_i = 11, 19,$ and 290 nM, respectively; for 5-HT_{2C}, $K_i = 85$ nM). This also limits the usefulness of this compound as a tool for exploring the effects of M_1 receptor agonism in vivo.

ADME Properties of 17. Compound **17** was investigated for its ADME properties in vitro and in vivo. Moderate plasma protein binding was found in both rats (52%) and humans (72%) following in vitro incubation studies. Intrinsic clearance in rat and human hepatocytes was determined to be 100 mL/min and 3.4 L/min, which is above the hepatic blood flow for both species (rat hepatic blood flow ~ 20 mL/min; human hepatic blood flow ~ 1.4 L/min). The high intrinsic clearance was in accordance with the observed in vivo pharmacokinetics in rats following intravenous and oral administration, where high systemic clearance and low oral bioavailability (F) was encountered. The plasma concentration–time profile is shown in Figure 5, and a summary of the pharmacokinetic parameter estimates is provided in Table 5. The ability of **17** to penetrate the blood–brain barrier was verified from analysis of plasma and brain homogenate samples after subcutaneous administration. From the AUCs, brain–plasma distribution ratios of 0.35 and 0.20 were found in mice and rats, and the data are shown in Figure 6.

When the results from intrinsic clearance, unbound fractions in plasma, and the in vivo clearance in rats were compared, the in vitro/in vivo extrapolated intravenous human hepatic clearance of **17** was predicted to be around 60 L/h (for a 70 kg subject) and hence below the human hepatic blood flow around 90 L/h. In vitro and in vivo evaluation of the series of analogues of **17** further suggests the possibility of reducing the human predicted systemic

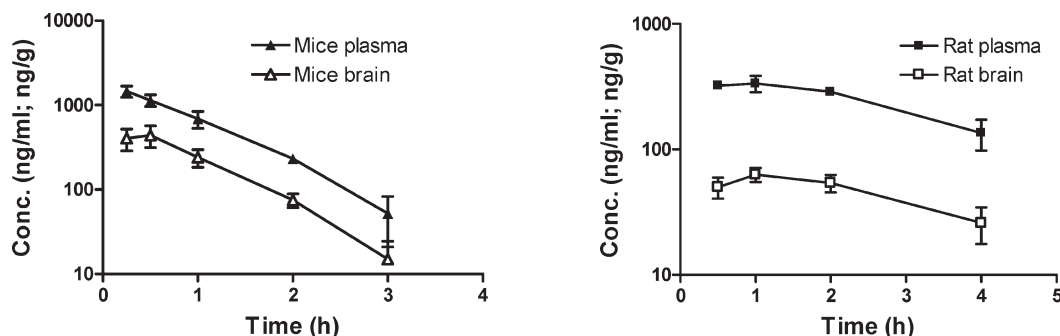


Figure 6. Plasma (ng/mL) and brain (ng/g) concentration–time courses of **17** following subcutaneous administration of 20 mg/kg (C57/6J mice) and 10 mg/kg (Sprague–Dawley rats). Each data point represents an average of $n = 3 \pm \text{SD}$.

clearance without compromising potency within this series of compounds. For example, compound **38** was found to have higher stability in human hepatocytes (1.2 L/min) compared to **17**, which in turn reduces the predicted human clearance by approximately 2-fold.

Effect in an in Vivo Model of Cognition: Delayed Alternation Y-Maze. To examine the effect of **17** on learning and memory, we tested the compound in the delayed alternation Y-maze task in mice. This task is applied to assess working memory and has previously been shown to be mediated by the prefrontal cortex and the hippocampus across species.^{31–33} In the Y-maze version, mice enter the maze from a fixed start arm and are forced to enter one goal arm to collect a reward (“sample run”). During the subsequent run, mice can choose between both goal arms (“choice run”); however, only the arm not entered previously is rewarded. Positive alternation between the two goal arms requires recollection of the previous arm entry, which is intact following a short time delay between the sample and choice run. As shown in Figure 7, a high degree of positive alternation (> 80%), interpreted as intact working memory, was achieved following a short delay (0 s). However, this memory was subject to a time-dependent memory decay, as evident by reduced alternation rates at chance level after a longer intertrail interval (ITI) of 60 s. Animals were treated with **17** or vehicle 30 min prior to a series of 20 alternation trials, applying both the short and long delay. Following the short delay, vehicle treated animals as well as all dose groups treated with **17** displayed high correct alternation rates (80–90%, data not shown). As expected, this performance was significantly lower and around chance levels in the vehicle group, following a 60 s delay (55.6 ± 5.3%) (Figure 7). In contrast, subjects treated with **17** showed a dose-dependent reversal of the delay-induced memory decay. Whereas pretreatment with lower doses, 0.31 and 1.3 mg/kg **17**, had no significant effect on alternation rates, groups treated with 10 and 20 mg/kg showed significantly increased levels of positive alternation compared to the vehicle treated group following the 60 s delay. As shown in Figure 6, systemic treatment of mice with 20 mg/kg **17** produced high brain exposures during the experiment (440 ± 127 ng/g after 30 min (= pretreatment time) and 240 ± 57 ng/g after 60 min (= end of experiment)). Equilibrium dialysis revealed about 70% nonspecific binding for compound **17** in mouse brain homogenates, which corresponds to a free concentration of 70 ng/mL (~170 nM) 60 min after dosing. Free brain concentrations of **17** were about 3-fold higher than the in vitro EC₅₀ value (61 nM) during the experiment, suggesting that the procognitive effect was achieved at concentrations that are relevant for an interaction with the M₁ receptor.

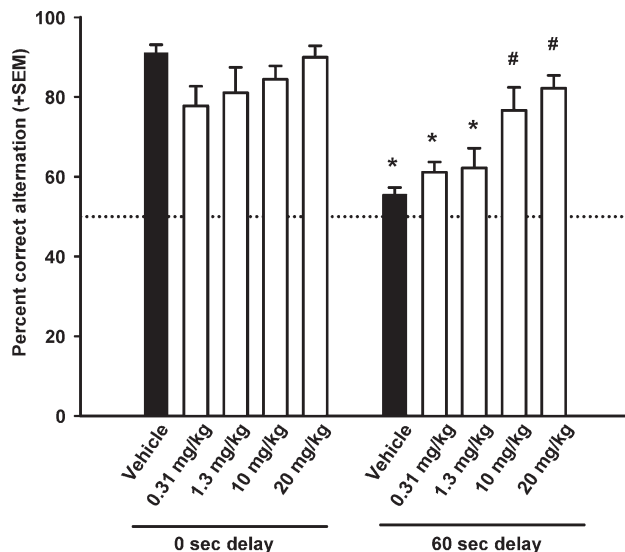


Figure 7. Compound **17** reverses delay-induced working memory decay in the mouse delayed alternation Y-maze task. The graph shows the percentage of positive alternation of arm entries in successive trial runs following a delay of 1 (“0 sec”) or 60 s. A two-way analysis of variance (ANOVA) with the all pairwise multiple comparison procedure (Student–Newman–Keuls method) revealed an overall difference for factor delay ($F = 45.150$; $p < 0.001$) and treatment ($F = 5.759$; $p < 0.001$). The vehicle group (black bars) displays a significant decline in correct alternation following the 60 s versus 0 s delay, as well as the low compound **17** dose groups (white bars) (veh, $p < 0.001$; 0.31 mg/kg, $p < 0.005$; 1.3 mg/kg, $p < 0.002$). Groups treated with 10 and 20 mg/kg **17** show a dose-dependent, significant increase in correct alternation following the 60 s delay compared to vehicle (10 mg/kg, $p < 0.003$; 20 mg/kg, $p < 0.001$). No differences were found between all groups within the 0 s delay (veh vs 0.31 mg/kg, $p = 0.152$; all others not tested). The dotted line indicates chance performance level (*, compared to the respective 0 s group; #, compared to the vehicle group at 60 s).

These data indicated that **17** dose-dependently reversed the delay-induced working memory decay in the delayed alternation Y-maze task in mice. Such procognitive effects support a pivotal role of M₁ receptors in learning and memory and a procognitive potential of compound **17**. A full pharmacological profile of **17**, including studies in schizophrenia relevant cognition models using perturbed animals, will be reported in a subsequent publication.

Conclusion

We have disclosed the discovery and SAR of a novel series of allosteric M₁ receptor agonists. The potent M₁ receptor agonist hit compound **5** displayed undesired agonistic activity

at the M₄ and M₅ receptors and was used as template for SAR investigations. It was revealed that equally potent and efficacious M₁ receptor agonists compounds as **5** could be found with much improved selectivity with respect to functional agonism at other muscarinic receptor subtypes. Compound **17** was prioritized within this series as a prototype compound, based on its selectivity for M₁ receptor functional agonism. It was demonstrated that **17** was an allosteric agonist at the M₁ receptor. In addition to its functional selectivity for the muscarinic M₁ receptor, **17** also had no binding affinity across the muscarinic receptor subtypes M₂–M₅. Likewise, a very limited cross-reactivity was observed toward a panel of 69 receptors, ion channels, transporters, and enzymes. Thus, **17** has an unprecedented overall selectivity for agonism at the M₁ receptor, making it an excellent compound for investigating the in vivo pharmacology of the M₁ receptor. We tested the compound in an in vivo model of learning and memory in mice and observed a dose-dependent procognitive effect on working memory. In vitro and in vivo characterization supported that **17** possesses acceptable pharmacokinetic properties. In addition, the potential for improving the metabolic stability within the series was established. Taken together, compound **17** is a high quality lead for a further drug discovery program aimed at identifying allosteric muscarinic M₁ receptor agonists. A detailed pharmacological profiling of this compound will be reported in a later publication.

Experimental Section

General Chemistry. The 500 MHz ¹H NMR spectra were recorded on a Bruker Avance AV-III-500 spectrometer. The 600 MHz ¹H NMR spectra were recorded on a Bruker Avance AV-III-600 spectrometer. Chemical shift values are expressed in ppm relative to Me₄Si.

Preparative HPLC purification with MS detection was performed on a Sciex API150ex preparative LC/MS system equipped with a Gilson 333 pump (master) and a Gilson 334 pump (slave) and an Applied Biosystems API150ex single quadrupole mass spectrometer with atmospheric pressure photoionization (APPI) ion source. The purities of the intermediates and final compounds were determined by integration of the UV signal obtained by analytical HPLC–UV–MS on a Sciex API150ex analytical LC/MS system equipped with 3 Shimadzu LC10ADvp LC pumps, a Shimadzu SPD-M20A photodiode array UV detector, and an Applied Biosystems API150ex single quadrupole mass spectrometer with an APPI ion source or by integration of the UV signal obtained by analytical HPLC–UV–MS on a Sciex API300 analytical LC/MS system equipped with 3 Shimadzu LC10ADvp LC pumps, an Acquity UPLC PDA detector with an analytical flow cell, and an Applied Biosystems API300 triple quadrupole mass spectrometer with an APPI ion source.

Chromatography was performed on silica gel 60 (230–400 mesh ASTM), Merck.

Strong cation exchange (SCX) chromatography columns (Bond-Elut, 500 mg/3 mL) were obtained from Varian.

TBD-methylpolystyrene is a polymer-bound version of the strong and highly hindered organic base 7-methyl-1,5,7-triazabicyclo[4.4.0]dec-5-ene (MTBD). The resin was obtained from Novabiochem, loading 2–3 mmol/g.

Reagents and solvents obtained from commercial sources were used without additional purification.

Xanomeline (**1**),¹³ AC-42 (**2**),³⁴ NDMC (**3**),²² and TBTP (**4**)³⁴ were prepared according to the cited literature procedures.

The purity of compounds, measured as described above, was > 95% unless otherwise stated.

3-(2-Fluoro-6-nitrophenyl)propionic Acid (39). Sodium hydride (60% oil dispersion) (112 mmol) was suspended in 110

mL of DMF and 50 mL of THF. Diethyl malonate (109 mmol) in 20 mL THF was added dropwise while maintaining the temperature of the reaction mixture below 40 °C. Then the mixture was stirred at ambient temperature for 2 h. 2-Fluoro-6-nitrobenzyl bromide (107 mmol) in 40 mL of DMF and 30 mL of THF was added dropwise while maintaining the temperature of the reaction mixture below 50 °C. The mixture was heated at reflux for 3 h and then stirred at ambient temperature for 18 h and poured onto brine. The reaction mixture was extracted with ethyl acetate, and the combined organic extracts were dried and evaporated under reduced pressure to yield a red oil. The oil was dissolved in 100 mL of glacial acetic acid, 50 mL of concentrated HCl, and 50 mL of H₂O and refluxed for 6 h. Then the mixture was stirred at room temperature for 18 h. The solvent was evaporated and the residue triturated with H₂O. The formed precipitate was filtered off and dissolved in 2 M NaOH and EtOH, each 400 mL. The mixture was refluxed for 40 min. Then the solvent volume was reduced to 500 mL. Ice (300 g) and 4 M HCl were added, to give acidic pH. The aqueous phase was extracted with ethyl acetate, and the organic fractions were combined, washed with brine, dried on MgSO₄, and evaporated. The crude was obtained as a dark solid and was used without further purification. Crude yield: 79%. ¹H NMR (DMSO-*d*₆, 500 MHz): 2.55 (t, 2H); 3.04 (t, 2H); 7.52–7.65 (2H); 7.82 (d, 1H); 12.38 (br s, 1H).

5-Fluoro-3,4-dihydro-1H-quinolin-2-one (7c). Intermediate **39** (9.4 mmol) was dissolved in 125 mL of MeOH. Then 250 mg of 10% Pd/C and HCOONH₄ (94 mmol) were added. The mixture was refluxed for 45 min. Then the mixture was cooled and filtered. The solvent was removed by evaporation. Toluene (50 mL) was added and removed by evaporation. The residue was partitioned between ethyl acetate and brine, and the aqueous phase was extracted with ethyl acetate. The combined organic fractions were washed with brine, dried, and filtered. The solvent was removed by evaporation, and the product was used without further purification. Crude yield: 96%. ¹H NMR (DMSO-*d*₆, 500 MHz): 2.47 (t, 2H); 2.87 (t, 2H); 6.70 (d, 1H); 6.77 (m, 1H); 7.16 (m, 1H).

6,7-Difluoro-3,4-dihydro-1H-quinolin-2-one (7g). 3,4-Difluorophenylamine (250 mmol) was dissolved in 500 mL of ethyl acetate, and triethylamine (300 mmol) was added. 3-Chloropropionyl chloride (275 mmol) was added dropwise while maintaining the temperature below 30 °C. The mixture was stirred at room temperature for 1 h, and then 250 mL of H₂O was added. The phases were separated, and the organic phase was washed with brine, dried on MgSO₄, and filtered. The solvent was evaporated and the obtained intermediate (120 mmol) was mixed well with aluminum trichloride (150 mmol) (caution: heating!) in a flask equipped with a washing flask containing 2 M NaOH. The resulting melt was heated at 180 °C for 1 h and then cooled and poured into ice–water. To the mixture were added 25 mL of concentrated HCl and 200 mL of dichloromethane. The obtained solid was recovered by filtration and dried. The crude product was recrystallized from ethyl acetate. Yield: 37%. ¹H NMR (DMSO-*d*₆, 500 MHz): 2.44 (t, 2H); 2.85 (t, 2H); 6.82 (m, 1H); 7.30 (m, 1H); 10.14 (br s, 1H).

6,7-Difluoro-4H-benzo[1,4]oxazin-3-one (7j). 4,5-Difluoro-2-nitrophenol (135 mmol) was dissolved in 250 mL of EtOH, and 2 g of 5% Pd/C was added. The mixture was hydrogenated at room temperature for 3 h in a Parr apparatus under 3 bar of H₂. The catalyst was filtered off and the solvent removed by evaporation. The residue was dissolved in 200 mL of DMF, and chloroacetyl chloride (209 mmol) was added with stirring. The mixture was stirred at room temperature for 18 h. Then K₂CO₃ (360 mmol) was added, and stirring was continued for another 24 h. The solvent was evaporated, and the residue was partitioned between H₂O and ethyl acetate. The phases were separated. The organic phase was dried on MgSO₄, and the solvent was removed by evaporation. Purification was by flash chromatography on silica using 40% ethyl acetate in heptane

as eluent. Yield: 70%. ^1H NMR (DMSO- d_6 , 500 MHz): 4.59 (s, 2H); 6.70 (dd, 1H); 7.15 (dd, 1H); 10.77 (br s, 1H).

4-(3-Bromopropyl)-4H-benzo[1,4]oxazin-3-one (8a). To a suspension of sodium hydride (60% in oil dispersion) (187 mmol) in 75 mL of DMF was added 4H-benzo[1,4]oxazin-3-one (170 mmol) in 100 mL of DMF at 10 °C. The mixture was stirred at room temperature for ~90 min and then poured into a ice-cooled solution of 1,3-dibromopropane in 100 mL of DMF with vigorous stirring. The mixture was stirred for ~15 min and then poured into 800 mL of brine. The aqueous phase was extracted with ethyl acetate, and the combined organic extracts were dried on MgSO_4 . After filtration the solvent was removed under reduced pressure and the crude product was purified by flash chromatography on silica using an eluent of 35% ethyl acetate in heptane. Yield: 62%. ^1H NMR (DMSO- d_6 , 500 MHz): 2.10 (qui, 2H); 3.59 (t, 2H); 4.02 (t, 2H); 4.65 (s, 2H); 6.99–7.10 (m, 3H); 7.23 (d, 1H).

N-{1-[3-(3-Oxo-2,3-dihydrobenzo[1,4]oxazin-4-yl)propyl]piperidin-4-yl}-2-phenylacetamide (17). Piperidin-4-ylcarbamic acid *tert*-butyl ester (18 mmol) and **8a** (18 mmol) were dissolved in 50 mL of MeCN, and K_2CO_3 (20 mmol) was added. The reaction mixture was stirred at 80 °C for 18 h, then cooled and poured into H_2O . The aqueous phase was extracted with ethyl acetate, and the combined organic extracts were dried on MgSO_4 and filtered. The solvent was removed under reduced pressure to yield an oil which was purified by flash chromatography on silica using 50% ethyl acetate in heptane as eluent. The obtained crude was dissolved in dichloromethane, and 15 mL of TFA/ H_2O (95:5) was added. After 20 min, more H_2O was added and to the solution was added 2 M NaOH to give a pH of ~12. The aqueous phase was extracted with ethyl acetate, the organic fractions were combined and dried on MgSO_4 , and the solvent was removed by evaporation to yield the intermediate 4-[3-(4-aminopiperidin-1-yl)propyl]-4H-benzo[1,4]oxazin-3-one as an oil. Yield: 50%. ^1H NMR (DMSO- d_6 , 500 MHz): 1.36 (m, 2H); 1.66 (m, 2H); 1.75 (m, 2H); 1.88 (t, 2H); 2.29 (t, 2H); 2.72 (m, 1H); 2.79 (m, 2H); 2.84 (t, 2H); 3.44 (m, 2H); 3.88 (t, 2H); 6.99 (t, 1H); 7.14–7.28 (3H).

The obtained intermediate (17 mmol) was dissolved in 60 mL of dry THF, and triethylamine (26 mmol) was added. The mixture was cooled to 5 °C, and phenylacetyl chloride (19 mmol) was added dropwise. The mixture was stirred at room temperature for 1 h and then filtered, and the solvent was removed in vacuo. The crude product was purified by flash chromatography on silica with gradient elution from 80% ethyl acetate in heptane (+5 vol % triethylamine) to 5% EtOH in ethyl acetate (+5 vol % triethylamine). Yield: 64%. ^1H NMR (DMSO- d_6 , 500 MHz): 1.39 (m, 2H); 1.67–1.73 (4H); 1.91 (t, 2H); 2.30 (t, 2H); 2.75 (m, 2H); 2.37 (s, 2H); 3.48 (m, 1H); 3.92 (t, 2H); 4.62 (s, 2H); 7.01 (d, 2H); 7.06 (m, 1H); 7.18–7.31 (5H); 7.99 (d, 1H).

Biological Methods. Cell Lines. Standard molecular cloning techniques³⁵ were used to generate the following cell lines: Chinese hamster ovary (CHO-K1) cells expressing either human muscarinic M_1 or M_2 receptor and baby hamster kidney cells (BHK-21) expressing human muscarinic M_3 , M_4 , M_5 , or M_1 Y381A receptors. Cell lines expressing M_2 and M_4 receptors coexpressed the promiscuous $\text{G}_{\alpha 16}$ subunit. The cell line was grown in DMEM or F-12 Kaighn's medium with L-glutamine (Gibco), 10% Fetal-Clone I serum (HyClone), and 1% penicillin and streptavidine and supplemented with appropriate antibiotics.

Calcium Mobilization Assays. Cells expressing muscarinic receptor were plated in growth medium at a density of 10 000 cells/well in clear-bottomed, poly-D-lysine coated 384-well plates (ArcticWhite LLC) and grown for 24 h at 37 °C in the presence of 5% CO_2 . Before assay, the cells were washed with assay buffer (Hanks' balanced salt solution with Ca^{2+} and Mg^{2+} (Gibco) containing 20 mM HEPES, pH 7.4). The cells were incubated with a calcium-sensitive fluorescent dye Calcium4 (Molecular Devices Inc.) with 2.5 mM Probenecid (Sigma) for 50 min at 37 °C followed by 10 min at room temperature. Calcium flux was measured using a Hamamatsu FDSS7000 imaging-based plate

reader (Hamamatsu Photonics) using 480 nm excitation light, and emitted fluorescent light passed through a 525 nm emission filter and was detected by a CCD camera. Test compounds were diluted in assay buffer from 2 mM stock solutions in 100% DMSO to give a 3× concentrated stock. Compounds were added to cells and fluorescence was measured at 1 Hz for 6 min starting just prior to compound addition. The fluorescence readout was calculated as max–min response, i.e., maximum fluorescence reading after and before liquid addition. The fluorescence max–min data were normalized to yield responses for no stimulation (buffer) and full stimulation (1 μM acetylcholine) of 0% and 100% stimulation, respectively. Concentration–response data were fitted to the four-parameter logistic equation to estimate compound potency (EC_{50}) and efficacy (E_{max}) of test compounds.²⁴ Schild regression experiments were performed by preincubating dye-loaded cells with increasing concentrations of the muscarinic antagonist atropine for 30 min, before the agonist response was assayed as described above. Schild regression analysis was performed by linear fitting to the following model: $\log(\text{dose ratio} - 1) = \log([\text{antagonist}]) - \log(K_d)$. If the 95% confidence interval of the slope included the value 1.0, the slope was estimated to unity and, hence, the agonist–antagonist interaction was defined as competitive.

Cell Membrane Preparation. Cells were grown in the appropriate medium to approximately 90% confluence. Cells were washed twice with 10 mL of PBS without Ca^{2+} , Mg^{2+} , and HCO_3^- . Cells were harvested in ice cold 20 mM HEPES/10 mM EDTA, pH 7.4, buffer and centrifuged at 3000g for 5 min. Cell pellets were frozen at –80 °C. The thawed pellet was resuspended in 20 mM HEPES/10 mM EDTA buffer, homogenized for 30 s with Ultra-Turrax T25 (IKA-Werke GmbH), and centrifuged at 1000g in 15 min at 4 °C. The supernatant was transferred to a new vial and centrifuged at 40000g for 30 min at 4 °C. The pellet was resuspended in 20 mM HEPES/0.1 mM EDTA, pH 7.4, and centrifuged at 40000g at 4 °C for 30 min. The pellet was resuspended in 20 mM HEPES/0.1 mM EDTA buffer/250 mM sucrose, and 1 mL aliquots were stored at –80 °C. Protein concentration was determined by BCA protein assay kit (Pierce).

Radioligand Binding Assays. Binding studies were performed by incubating test compound (25 μL), cell membrane preparation (25 μL , typically 5 μg of protein/well) with radioligand (25 μL), and 25 μL of wheat germ agglutinin SPA beads (0.25 mg/well, GE Healthcare) in a white Wallac 96-well isoplate with clear bottom (PerkinElmer). The reagents were mixed for 90 min on an orbital shaker and then centrifuged at 1500 rpm for 5 min at room temperature. Plates were counted in a Wallac TriLux 1450 Microbeta for 2 min/well. Assay buffer was 12.5 mM sodium phosphate buffer with 2 mM NiCl_2 , 2.5 mM MgCl_2 , pH 7.4. The total binding, which comprised less than 5% of added radioligand, was defined by assay buffer, whereas the nonspecific binding was defined in the presence of 1 μM atropine. The nonspecific binding constituted ~5% of the total binding. The following radioligands were used: M_2 , 3.0 nM ^3H -AFDX-384 (PerkinElmer); M_3 – M_5 , 0.3 nM ^3H -4-DAMP (PerkinElmer). Data points were expressed as percent of the specific binding, and the IC_{50} values were determined by nonlinear regression analysis using a sigmoidal variable slope curve fitting. The dissociation constant (K_i) was calculated from the Cheng–Prusoff equation ($K_i = \text{IC}_{50}/(1 + (L/K_d))$), where the concentration of free radioligand L is approximated to the concentration of added radioligand in the assay and K_d equals the affinity of the radioligand to the receptor.

Broad Pharmacology Profiling. Broad profiling was performed by CEREP (France). Compounds were generally assayed for the ability to displace radioligand binding to the assayed targets. The following targets were profiled by enzyme assays: PDE3,4,5, Lyn kinase, p38 α kinase, and acetylcholine esterase. Compounds were tested at 10 μM , $n = 2$, at the following targets (CEREP catalog number in parentheses): D_1 (no. 803-1h), D_{25}

(no. 803-2h), H₃ (no. 805-3h), rolipram (no. 833), μ (MOP, agonist site) (no. 843-h), MC₄ (no. 889-4h), β_1 (no. 802-2ah), 5-HT_{1A} (no. 808-1ah), 5-HT_{2B} (agonist site) (no. 808-2bah), 5-HT_{2A} (agonist site) (no. 808-2ah), Na⁺ channel (site 2) (no. 862-a), H₁ (no. 805-1h), PCP (no. 895-6), glucocorticoid (GR) (no. 812-h), σ (nonselective) (no. 891), D_{2S} (agonist site) (no. 803-2ha), M₄ (no. 806-4h), GABA_A (no. 804-1), α_{2A} (no. 802-1bAh), ETA (no. 825-1h), 5-HT_{4c} (no. 808-4eh), DA transporter (no. 803-Uh), D_{4.4} (no. 803-44h), M₁ (no. 806-1h), α_1 (non-selective) (no. 802-1a), A₁ (no. 801-1h), BZD (central) (no. 851), M₂ (no. 806-2h), M₃ (no. 806-3h)

N (neuronal) (α -BGTX-insensitive) ($\alpha_4\beta_2$) (no. 807-n1), A₁ (agonist site) (no. 801-1ah), MT₁ (no. 892-1h), Ca²⁺ channel (L, diltiazem site) (benzothiazepines) (no. 861-L2), α_{2B} (no. 802-1bBc), κ (KOP) (no. 842), 5-HT_{2C} (agonist site) (no. 808-8cha), 5-HT₇ (no. 808-7h), D₃ (no. 803-3h), CCKB (CCK2) (no. 824-2h), MAO-A (no. 838-a), β_2 (no. 802-2bh), Ca²⁺ channel (L, verapamil site) (phenylalkylamines) (no. 861-L3), H₂ (no. 805-2hc), ML₂ (MT₃) (no. 892-2), M5 (no. 806-5h), choline transporter (CHT₁) (no. 806-Uh), I₁ (no. 809-1p), NK₁ (no. 826-1h), Y₁ (no. 827-1h), N (muscle-type) (no. 807-mh), 5-HT transporter (no. 808-Uh), CB₁ (no. 835-ch), 5-HT_{1B} (no. 808-1b), NE transporter (no. 802-Uh), Ca²⁺ channel (N) (no. 861-N), GABA transporter (no. 804-U), A₃ (no. 801-3h), NK₂ (no. 826-2h), δ_2 (DOP) (no. 841-h), Ca²⁺ channel (L, DHP site) (no. 861-L1), 5-HT₃ (no. 808-3h), UT₁ (no. 853-hc), A_{2A} (no. 801-2ah).

In Vitro ADME Assays. Hepatocyte Clearance Determination. The intrinsic clearance of compounds in hepatocytes were determined by the $t_{1/2}$ method,³⁶ i.e., measurement of the disappearance of 1 μ M compound over time by LC/MS–MS. Pooled male rat cryopreserved hepatocytes (Sprague–Dawley) and pooled cryopreserved human hepatocytes from 10 donors (male and female) from CellzDirect, Inc., Durham, NC, were used. Cells were thawed in a 37 °C water bath and live cells counted and seeded in a total of 100 μ L in Dulbecco's modified Eagle medium (high glucose) with 5 mM HEPES buffer in 96-well plates. Then 250 000 and 500 000 cells/mL were used for rat and human hepatocytes, respectively. Incubations were started after 15 min of preincubation and stopped at time points 0, 5, 15, 30, and 60 min for rats and 0, 30, 60, 90, and 120 min for human hepatocytes. The $t_{1/2}$ is scaled to intrinsic clearance values of L/min for humans and mL/min for rats. Values of scaling factors are 135/120 million cells per gram of liver, 45/20 g of liver per kilogram, and standard weight of 0.25/70 kg for rat and human, respectively.

Protein Binding. Plasma protein binding was determined in vitro in rat and human serum following incubation of 0.1 μ M test compound dissolved in PBS in ultracentrifugation filter plates (300 μ L in each well) (Multiscreen filter plates, 10 kDa MW cutoff, Millipore) for 60 min at 37 °C. Plates were then centrifuged for 60 min at 37 °C (3200 rcf), and the free fraction was measured by LC/MS–MS following addition of internal standard.

Nonspecific binding in brain were obtained by equilibrium dialysis in 96-well format. Freshly isolated mouse brains were homogenized twice in two volumes of phosphate buffer, pH 7.4. The dialysis methodology was modified from ref 37. Membranes (cutoff 12–14 kDa, HTDialysis) was soaked in PBS/ethanol 80:20 and rinsed in deionized water before use. Brain homogenate was spiked with test compound to a final concentration of 1 μ M, and equilibrium dialysis was performed by incubating at 37 °C for 5 h. Subsequently, the compound concentration was measured in the buffer phase.

In Vivo ADME Studies. All dosing solutions consisted of 5% HP- β -cyclodextrin, pH 5. Serial blood sampling from the tail vein in awake rats was used for pharmacokinetic assessment following intravenous (1 mg/kg) and oral (2 mg/kg) drug administration. For brain/plasma exposure studies, cardiac blood was obtained under isoflurane anesthesia. Dose volumes of 5 and 10 mL/kg were applied for rats and mice, respectively. Blood samples were collected in EDTA-coated tubes and cen-

trifuged for 10 min at 4 °C after which plasma was drawn off. Following decapitation, the brain was removed and stored at –80 °C pending bioanalysis.

Plasma and Brain Bioanalysis. Brain homogenate was prepared by homogenizing the whole brain with 70% acetonitrile (1:4 v/v) followed by centrifugation and collection of the supernatant. Plasma and brain supernatant samples were frozen at –80 °C until analysis. Concentrations of were determined in plasma and brain homogenate using turboflow chromatography (dual column, focus mode, Cohesive Technologies, U.K.) followed by MS/MS detection in positive-ion electrospray ionization mode (Sciex API-3000 MS, Applied Biosystems, The Netherlands). Samples of plasma and brain homogenate were prepared by adding an equal amount of 10% methanol with internal standard included (escitalopram), and after centrifugation (6000g, 5 °C, 20 min) an amount of 10 μ L was injected into the turboflow system. The mobile phase consisted of water/methanol with 0.1% ammonium hydroxide pumped as a gradient through an XTerra analytical column (MS C8, 2.1 mm \times 20 mm, Waters Corp., MA). The lower limit of quantification was typically 0.5 ng/mL in plasma and 5 ng/g in brain.

In Vitro/in Vivo Extrapolation of Clearance. According to the well-stirred model,²⁵ an approximate hepatic clearance in each species (CL_{pred}) was predicted from hepatocyte intrinsic clearance (CL_{int}) according to

$$CL_{pred} = \frac{LBF \times CL_{int} \times f_u}{LBF + CL_{int} \times f_u}$$

where LBF is hepatic blood flow and f_u is the fraction unbound in serum. Human clearance was then estimated from the observed in vivo rat clearance and the in vitro clearance prediction in each species ($CL_{pred, human}$, $CL_{pred, rat}$)²⁶ according to

$$CL_{human} = CL_{rat} \frac{CL_{pred, human}}{CL_{pred, rat}}$$

Delayed Alternation. Y-Maze. Ten male C57Bl/6J mice (22–24 g, Charles River, Germany) were used for the delayed alternation Y-maze. The maze consisted of gray, nontransparent Plexiglas, shaped to a Y with each arm arranged in 120° to each other and measuring 32 cm \times 7 cm \times 8 cm. One arm was designated as “start arm”, and the two remaining were “goal arms”. The maze was mounted on an airflow table. Each arm was equipped with a guillotine door allowing restriction to the start arm or providing entrance into each goal arm. Both goal arms were equipped with a small cup at the end of the arm that was baited with 15 μ L of chocolate milk (Cocio, Denmark). Before drug testing, subjects were trained to the alternation procedure until an 80% correct alternation rate was reached following the 1s ITI. Subsequently, animals were subjected to drug testing, where 1 s (designated “0 sec”) and 60 s delays were assigned randomly. Subjects were individually placed in the start arm and given a “sample run”, during which one of the goal arms was blocked. Once the subject collected the reward, it was returned manually to the start arm and restricted there for the delay. During the following run (“choice run”) both arms were accessible, but the subject was rewarded only when entering the goal arm opposite that visited during the sample run (i.e., the arm visited during sample run was not rebaited). The animal was returned to the start arm and restricted there for 10 s after which a new trial consisting of sample and choice run started. A total of 20 trials were performed per day and mouse (10 \times 0 s delay, 10 \times 60 s delay). For drug testing, animals were assigned to a Latin-square design in which each mouse was tested in each dose group over 1 week of testing. Lu AE51090 and vehicle (10% HP- β -cyclodextrin) were dosed subcutaneously in a volume of 5 mL/kg and 30 min before the experiment. Data are expressed as the mean \pm SEM. Significant differences between group mean values were assessed by two-way analysis of variance

(ANOVA) with the all pairwise multiple comparison procedure (Student–Newman–Keuls method) (SigmaStat 3.0, SPSS).

All *in vivo* experiments were performed in accordance with Danish legislation, and animals were treated with adherence to guidelines for the care of experimental animals.

Supporting Information Available: Synthesis procedures, spectroscopic data, and purities for intermediates **8b–k** and compounds **5**, **6**, **9–16**, and **18–38**. This material is available free of charge via the Internet at <http://pubs.acs.org>.

References

- Caulfield, M. P. Muscarinic receptors—characterization, coupling, function. *Pharmacol. Ther.* **1993**, *58*, 319–379.
- Davies, P.; Maloney, A. J. Selective loss of central cholinergic neurons in Alzheimer's disease. *Lancet* **1976**, *2*, 1403.
- Muir, J. L. Acetylcholine, aging, and Alzheimer's disease. *Pharmacol., Biochem. Behav.* **1997**, *56*, 687–696.
- Wess, J. Muscarinic acetylcholine receptor knockout mice: novel phenotypes and clinical implications. *Annu. Rev. Pharmacol. Toxicol.* **2004**, *44*, 423–450.
- Anagnostaras, S. G.; Murphit, G. G.; Hamilton, S. E.; Mitchell, S. L.; Rahnama, N. P.; Nathanson, N. M.; Silva, A. J. Selective cognitive dysfunction in acetylcholine M1 muscarinic receptor mutant mice. *Nat. Neurosci.* **2003**, *6*, 51–58.
- Dean, B.; McLeod, M.; Keriakous, D.; McKenzie, J.; Scarr, E. Decreased muscarinic 1 receptors in the dorsolateral prefrontal cortex of subjects with schizophrenia. *Mol. Psychiatry* **2002**, *7*, 1083–1091.
- Mancama, D.; Arrantz, M. J.; Landau, S.; Kerwin, R. Reduced expression of the muscarinic 1 receptor cortical subtype in schizophrenia. *Am. J. Med. Genet., Part B* **2003**, *119*, 2–6.
- Langmead, C. J.; Watson, J.; Reavill, R. Muscarinic acetylcholine receptors as CNS drug targets. *Pharmacol. Ther.* **2008**, *117*, 232–243.
- Sur, C.; Kinney, G. G. Selective targeting of muscarinic receptors: novel therapeutic approaches for psychotic disorders. *Curr. Neuropharmacol.* **2005**, *3*, 63–71.
- Sellin, A. K.; Shad, M.; Tamminga, C. Muscarinic agonists for the treatment of cognition in schizophrenia. *CNS Spectrums* **2008**, *13*, 985–996.
- Fischer, A. Cholinergic treatments with emphasis on m1 muscarinic agonists as potential disease-modifying agents for Alzheimer's disease. *Neurotherapeutics* **2008**, *5*, 433–442.
- Fischer, A. Muscarinic receptor agonists in Alzheimer's disease. *CNS Drugs* **1999**, *12*, 197–214.
- Sauerberg, P.; Olesen, P. H.; Nielsen, S.; Treppendahl, S.; Sheardown, M. J.; Honore, T.; Mitch, C. H.; Ward, J. S.; Pike, A. J. Novel functional M1 selective muscarinic agonists. Synthesis and structure–activity relationships of 3-(1,2,5-thiadiazolyl)-1,2,5,6-tetrahydro-1-methylpyridines. *J. Med. Chem.* **1992**, *35*, 2274–2283.
- Bodick, N. C.; Offen, W. W.; Levey, A. I.; Cutler, N. R.; Gauthier, S. G.; Satlin, A.; Shannon, H. E.; Tollefson, G. D.; Rasmussen, K.; Bymaster, F. P.; Hurley, D. J.; Potter, W. Z.; Paul, S. M. Effects of xanomeline, a selective muscarinic receptor agonist, on cognitive function and behavioural symptoms in Alzheimer disease. *Arch. Neurol.* **1997**, *54*, 465–473.
- Bymaster, F. P.; Whitesitt, C. A.; Shannon, H. E.; DeLapp, N.; Ward, J. S.; Calligaro, D. O.; Shipley, L. A.; Buelke-Sam, J. L.; Bodick, N. C.; Farde, L.; Sheardown, M. J.; Olesen, P. H.; Hansen, K. T.; Suzdak, P. D.; Swedberg, M. D. B.; Sauerberg, P.; Mitch, C. H. Xanomeline: a selective muscarinic agonist for the treatment of Alzheimer's disease. *Drug Dev. Res.* **1997**, *40*, 158–170.
- Shekar, A.; Potter, W. Z.; Lightfoot, J.; Lienemann, J.; Dubé, S.; Mallinckrodt, C.; Bymaster, F. P.; McKinzie, D. L.; Felder, C. C. Selective muscarinic receptor agonist xanomeline as a novel treatment approach for schizophrenia. *Am. J. Psychiatry* **2008**, *165*, 1033–1039.
- Moltzen, E. K.; Bjørnholm, B. Medicinal chemistry of muscarinic agonists: developments since 1990. *Drugs Future* **1995**, *20*, 37–54.
- Heinrich, J. N.; Butera, J. A.; Carrick, T.; Kramer, A.; Kowal, D.; Lock, T.; Marquis, K. L.; Paush, M. H.; Popiolek, M.; Sun, S.-C.; Tseng, E.; Uveges, A. J.; Mayer, S. C. Pharmacological comparison of muscarinic ligands: historical versus more recent muscarinic M₁-preferring receptor agonists. *Eur. J. Pharmacol.* **2009**, *605*, 53–56.
- Spalding, T. A.; Trotter, C.; Skjærbaek, N.; Messier, T. L.; Currier, E. A.; Burstein, E. S.; Li, D.; Hacksell, U.; Brann, M. R. Discovery of an ectopic activation site on the M₁ muscarinic receptor. *Mol. Pharmacol.* **2002**, *61*, 1297–1302.
- Spalding, T. A.; Ma, J.-N.; Ott, T. R.; Friberg, M.; Bajpai, A.; Bradley, S. R.; Davis, R. E.; Brann, M. R.; Burstein, E. S. Structural requirements of transmembrane domain 3 for activation by the muscarinic receptor agonists AC-42, AC-260484, clozapine, and *N*-desmethylozapine: evidence for three distinct modes of receptor activation. *Mol. Pharmacol.* **2006**, *70*, 1974–1983.
- Langmead, C. J.; Fry, V. A. H.; Forbes, I. T.; Branch, C. L.; Christopoulos, A.; Wood, M. D.; Herdon, H. J. Probing the molecular mechanism of interaction between AC-42 and the muscarinic M₁ receptor: direct pharmacological evidence that AC-42 is an allosteric agonist. *Mol. Pharmacol.* **2006**, *69*, 236–246.
- Blatter, F.; Thygesen, M. B.; Tolf, B.-R.; Berghausen, J. Method of Synthesis and Isolation of Solid *N*-Desmethylozapine and Crystalline Forms Thereof. US 2005282800, 2005.
- Bridges, T. M.; Brady, A. E.; Kennedy, J. P.; Daniels, R. N.; Miller, N. R.; Kwango, K.; Breiniger, M. L.; Gentry, P. R.; Brogan, J. T.; Jones, C. K.; Conn, P. J.; Lindsley, C. W. Synthesis and SAR of analogues of the M1 allosteric agonist TBPB. Part I: Exploration of alternative benzyl and privileged structure moieties. *Bioorg. Med. Chem. Lett.* **2008**, *18*, 5439–5442.
- Motulsky, H.; Christopoulos, A. *Fitting Models to Biological Data Using Linear and Nonlinear Regression*; Oxford University Press: Oxford, U.K., 2004.
- Rowland, M.; Tozer, T. N. *Clinical Pharmacokinetics: Concepts and Applications*; Williams and Wilkins: Baltimore, MD, 1995.
- Lave, T.; Coassolo, P.; Reigner, B. Prediction of hepatic metabolic clearance based on interspecies allometric scaling techniques and *in vitro*–*in vivo* correlations. *Clin. Pharmacokinet.* **1999**, *36*, 211–231.
- Mirza, N. R.; Peters, D.; Sparks, R. G. Xanomeline and the antipsychotic potential of muscarinic receptor subtype selective agonists. *CNS Drug Rev.* **2003**, 159–186.
- Jones, C. K.; Brady, A. E.; Bubser, M.; Deutch, A. Y.; Williams, L. C. TBPB is a highly selective M₁ allosteric muscarinic receptor agonist *in vitro* and produces robust antipsychotic-like effects *in vivo*. *Neuropsychopharmacology* **2006**, *31*, S116.
- Langmead, C. J.; Christopoulos, A. Allosteric agonists of 7TM receptors: expanding the pharmacological toolbox. *Trends Pharmacol. Sci.* **2006**, *27*, 475–481.
- Sur, C.; Mallorga, P. J.; Wittmann, M.; Jacobson, M. A.; Pascarella, D.; Williams, J. B.; Brandish, P. E.; Pettibone, D. J.; Scolnick, E. M.; Conn, P. J. *N*-Desmethylozapine, an allosteric agonist at muscarinic 1 receptor, potentiates *N*-methyl-D-aspartate receptor activity. *Proc. Natl. Acad. Sci. U.S.A.* **2003**, *100*, 13674–13679.
- Aultman, J. M.; Moghaddam, B. Distinct contributions of glutamate and dopamine receptors to temporal aspects of rodent working memory using a clinically relevant task. *Psychopharmacology* **2001**, *153*, 353–364.
- Courtney, S. M.; Petit, L.; Maisog, J. M.; Ungerleider, L. G.; Haxby, J. V. An area specialized for spatial working memory in human frontal cortex. *Science* **1998**, *279*, 1347–1351.
- Kesner, R. P.; Hunt, M. E.; Williams, J. M.; Long, J. M. Prefrontal cortex and working memory for spatial response, spatial location, and visual object information in the rat. *Cereb. Cortex* **1996**, *6*, 311–318.
- Brann, M.; Messier, T.; Currier, E.; Duggento, K.; Friberg, M.; Skjærbaek, N.; Spalding, T. Compounds with activity on muscarinic receptors, WO200105763, 2001.
- Sambrook, J.; Fritsch, E. F.; Maniatis, T. *Molecular Cloning: A Laboratory Manual*; Cold Spring Harbor Laboratory Press: Cold Spring Harbor, NJ, 1989.
- Obach, R. S.; Baxter, J. G.; Liston, T. E.; Silber, B. M.; Jones, B. C.; MacIntyre, F.; Rance, D. J.; Wastall, P. The prediction of human pharmacokinetic parameters from preclinical and *in vitro* metabolism data. *J. Pharmacol. Exp. Ther.* **1997**, *283*, 46–58.
- Kalvass, J. C.; Maurer, T. S. Influence of nonspecific brain and plasma binding on CNS exposure: implications for rational drug discovery. *Biopharm. Drug Dispos.* **2002**, *23*, 327–338.